A measurement of the forward-backward asymmetry of $e^+e^- \to c\bar{c}$ and $e^+e^- \to b\bar{b}$ at centre of mass energies on and near the Z^0 peak using $D^{*\pm}$ mesons

OPAL Collaboration

R. Akers[16], G. Alexander[23], J. Allison[16], K.J. Anderson[9], S. Arcelli[2], A. Astbury[28], D. Axen[29], G. Azuelos[18,a],
J.T.M. Baines[16], A.H. Ball[17], J. Banks[16], R.J. Barlow[16], S. Barnett[16], R. Bartoldus[3], J.R. Batley[5], G. Beaudoin[18],
A. Beck[23], G.A. Beck[13], J. Becker[10], C. Beeston[16], T. Behnke[27], K.W. Bell[20], G. Bella[23], P. Bentkowski[18], P. Berlich[10],
S. Bethke[11], O. Biebel[3], I.J. Bloodworth[1], P. Bock[11], B. Boden[3], H.M. Bosch[11], M. Boutemeur[18], H. Breuker[8,b],
P. Bright-Thomas[25], R.M. Brown[20], A. Buijs[8], H.J. Burckhart[8], C. Burgard[27], P. Capiluppi[2], R.K. Carnegie[6],
A.A. Carter[13], J.R. Carter[5], C.Y. Chang[17], D.G. Charlton[8], S.L. Chu[4], P.E.L. Clarke[15], J.C. Clayton[1], I. Cohen[23],
J.E. Conboy[15], M. Cooper[22], M. Coupland[14], M. Cuffiani[2], S. Dado[22], G.M. Dallavalle[2], S. De Jong[13],
L.A. del Pozo[5], H. Deng[17], A. Dieckmann[11], M. Dittmar[4], M.S. Dixit[7], E. do Couto e Silva[12], J.E. Duboscq[8],
E. Duchovni[26], G. Duckeck[11], I.P. Duerdoth[16], D.J.P. Dumas[6], P.A. Elcombe[5], P.G. Estabrooks[6], E. Etzion[23],
H.G. Evans[9], F. Fabbri[2], B. Fabbro[21], M. Fierro[2], M. Fincke-Keeler[28], H.M. Fischer[3], D.G. Fong[17], M. Foucher[17],
A. Gaidot[21], J.W. Gary[4], J. Gascon[18], N.I. Geddes[20], C. Geich-Gimbel[3], S.W. Gensler[9], F.X. Gentit[21],
G. Giacomelli[2], R. Giacomelli[2], V. Gibson[5], W.R. Gibson[13], J.D. Gillies[20], J. Goldberg[22], D.M. Gingrich[30,a],
M.J. Goodrick[5], W. Gorn[4], C. Grandi[2], F.C. Grant[5], J. Hagemann[27], G.G. Hanson[12], M. Hansroul[8], C.K. Hargrove[7],
P.F. Harrison[13], J. Hart[8], P.M. Hattersley[1], M. Hauschild[8], C.M. Hawkes[8], E. Heflin[4], R.J. Hemingway[6],
G. Herten[10], R.D. Heuer[8], J.C. Hill[5], S.J. Hillier[8], T. Hilse[10], D.A. Hinshaw[18], J.D. Hobbs[8], P.R. Hobson[25],
D. Hochman[26], R.J. Homer[1], A.K. Honma[28,a], R.E. Hughes-Jones[16], R. Humbert[10], P. Igo-Kemenes[11], H. Ihssen[11],
D.C. Imrie[25], A.C. Janissen[6], A. Jawahery[17], P.W. Jeffreys[20], H. Jeremie[18], M. Jimack[1], M. Jones[29], R.W.L. Jones[8],
P. Jovanovic[1], C. Jui[4], D. Karlen[6], K. Kawagoe[24], T. Kawamoto[24], R.K. Keeler[28], R.G. Kellogg[17], B.W. Kennedy[15],
J. King[13], S. Kluth[5], T. Kobayashi[24], D.S. Koetke[8], T.P. Kokott[3], S. Komamiya[24], J.F. Kral[8], R. Kowalewski[8],
J. von Krogh[11], J. Kroll[9], P. Kyberd[13], G.D. Lafferty[16], H. Lafoux[21], R. Lahmann[17], J. Lauber[8], J.G. Layter[4],
P. Leblanc[18], A.M. Lee[31], E. Lefebvre[18], M.H. Lehto[15], D. Lellouch[26], C. Leroy[18], J. Letts[4], L. Levinson[26],
S.L. Lloyd[13], F.K. Loebinger[16], J.M. Lorah[17], B. Lorazo[18], M.J. Losty[7], X.C. Lou[12], J. Ludwig[10], A. Luig[10],
M. Mannelli[8], S. Marcellini[2], C. Markus[3], A.J. Martin[13], J.P. Martin[18], T. Mashimo[24], P. Mättig[3], U. Maur[3],
J. McKenna[29], T.J. McMahon[1], J.R. McNutt[25], F. Meijers[8], D. Menszner[11], F.S. Merritt[9], H. Mes[7], A. Michelini[8],
R.P. Middleton[20], G. Mikenberg[26], J. Mildenberger[6], D.J. Miller[15], R. Mir[12], W. Mohr[10], C. Moisan[18],
A. Montanari[2], T. Mori[24], M. Morii[24], U. Müller[3], B. Nellen[3], H.H. Nguyen[9], S.W. O'Neale[1], F.G. Oakham[7],
F. Odorici[2], H.O. Ogren[12], C.J. Oram[28,a], M.J. Oreglia[9], S. Orito[24], J.P. Pansart[21], B. Panzer-Steindel[8],
P. Paschievici[26], G.N. Patrick[20], N. Paz-Jaoshvili[23], M.J. Pearce[1], P. Pfister[10], J.E. Pilcher[9], J. Pinfold[30], D. Pitman[28],
D.E. Plane[8], P. Poffenberger[28], B. Poli[2], T.W. Pritchard[13], H. Przysiezniak[18], G. Quast[27], M.W. Redmond[8],
D.L. Rees[8], G.E. Richards[16], M. Rison[5], S.A. Robins[5], D. Robinson[8], A. Rollnik[3], J.M. Roney[28], E. Ros[8],
S. Rossberg[10], A.M. Rossi[2], M. Rosvick[28], P. Routenburg[30], K. Runge[10], O. Runolfsson[8], D.R. Rust[12], M. Sasaki[24],
C. Sbarra[2], A.D. Schaile[26], O. Schaile[10], W. Schappert[6], F. Scharf[3], P. Scharff-Hansen[8], P. Schenk[4], J. Schneps[22,d],
B. Schmitt[3], H. von der Schmitt[11], M. Schröder[12], C. Schwick[27], J. Schwiening[3], W.G. Scott[20], M. Settles[12],
T.G. Shears[5], B.C. Shen[4], C.H. Shepherd-Themistocleous[7], P. Sherwood[15], G.P. Siroli[2], A. Skillman[16], A. Skuja[17],
A.M. Smith[8], T.J. Smith[28], G.A. Snow[17], R. Sobie[28], R.W. Springer[17], M. Sproston[20], A. Stahl[3], C. Stegmann[10],
K. Stephens[16], J. Steuerer[28], R. Ströhmer[11], D. Strom[19], H. Takeda[24], T. Takeshita[24,c], S. Tarem[26], M. Tecchio[9],
P. Teixeira-Dias[11], N. Tesch[3], M.A. Thomson[15], E. Torrente-Lujan[22], S. Towers[28], G. Transtromer[25], N.J. Tresilian[16],
T. Tsukamoto[24], M.F. Turner[8], D. Van den plas[18], R. Van Kooten[27], G.J. VanDalen[4], G. Vasseur[21], A. Wagner[27],
D.L. Wagner[9], C. Wahl[10], C.P. Ward[5], D.R. Ward[5], P.M. Watkins[1], A.T. Watson[1], N.K. Watson[8], M. Weber[11],
P. Weber[6], P.S. Wells[8], N. Wermes[3], M.A. Whalley[1], B. Wilkens[10], G.W. Wilson[4], J.A. Wilson[1], V-H. Winterer[10],
T. Wlodek[26], G. Wolf[26], S. Wotton[11], T.R. Wyatt[16], R. Yaari[26], A. Yeaman[13], G. Yekutieli[26], M. Yurko[18],
W. Zeuner[8], G.T. Zorn[17]

[1] School of Physics and Space Research, University of Birmingham, Birmingham, B15 2TT, UK
[2] Dipartimento di Fisica dell' Università di Bologna and INFN, I-40126 Bologna, Italy
[3] Physikalisches Institut, Universität Bonn, D-53115 Bonn 1, Germany
[4] Department of Physics, University of California, Riverside, CA92521, USA
[5] Cavendish Laboratory, Cambridge, CB3 0HE, UK
[6] Carleton University, Department of Physics, Colonel By Drive, Ottawa, Ontario K1S 5B6, Canada

[7] Centre for Research in Particle Physics, Carleton University, Ottawa, Ontario K1S 5B6, Canada
[8] CERN, European Organisation for Particle Physics, CH-1211 Geneva 23, Switzerland
[9] Enrico Fermi Institute and Department of Physics, University of Chicago, Chicago IL60637, USA
[10] Fakultät für Physik, Albert Ludwigs Universität, D-79104 Freiburg, Germany
[11] Physikalisches Institut, Universität Heidelberg, D-69120 Heidelberg, Germany
[12] Indiana University, Department of Physics, Swain Hall West 117, Bloomington, IN 47405, USA
[13] Queen Mary and Westfield College, University of London, London, E1 4NS, UK
[14] Birkbeck College, London, WC1E 7HV, UK
[15] University College London, London, WC1E 6BT, UK
[16] Department of Physics, Schuster Laboratory, The University, Manchester, M13 9PL, UK
[17] Department of Physics, University of Maryland, College Park, MD 20742, USA
[18] Laboratoire de Physique Nucléaire, Université de Montréal, Montréal, Quebec, H3C 3J7, Canada
[19] University of Oregon, Department of Physics, Eugene, OR 97403, USA
[20] Rutherford Appleton Laboratory, Chilton, Didcot, Oxfordshire, OX11 0QX, UK
[21] DAPNIA/SPP, Saclay, F-91191 Gif-sur-Yvette, France
[22] Department of Physics, Technion-Israel Institute of Technology, Haifa 32000, Israel
[23] Department of Physics and Astronomy, Tel Aviv University, Tel Aviv 69978, Israel
[24] International Centre of Elementary Particle Physics and Department of Physics, University of Tokyo, Tokyo 113, and Kobe University, Kobe 657, Japan
[25] Brunel University, Uxbridge, Middlesex, UB8 3PH UK
[26] Nuclear Physics Department, Weizmann Institute of Science, Rehovot, 76100, Israel
[27] Universität Hamburg/DESY, II Institut für Experimental Physik, D-22603 Hamburg, Germany
[28] University of Victoria, Department of Physics, PO Box 3055, Victoria BC V8W 3P6, Canada
[29] University of British Columbia, Department of Physics, Vancouver BC V6T 1Z1, Canada
[30] University of Alberta, Department of Physics, Edmonton AB T6G 2N5, Canada
[31] Duke University, Department of Physics, Durham, NC 27708-0305, USA

Abstract. A measurement is presented of the forward-backward asymmetry of the processes $e^+e^+ \to c\bar{c}$ and $e^+e^+ \to b\bar{b}$ at centre of mass energies near 91 GeV. Decays of the Z^0 into charm and bottom quarks are identified using 6507 charged D^* mesons, reconstructed in the decays $D^{*\pm} \to D^0\pi^\pm \to (K^\mp\pi^\pm)\pi^\pm$, $D^{*\pm} \to D^0\pi^\pm \to (K^\mp\pi^\pm\pi^0)\pi^\pm$ and $D^{*\pm} \to D^0\pi^\pm \to (K^\mp\pi^\pm\pi^\mp\pi^\pm)\pi^\pm$. The c quark asymmetry on the Z^0 peak is measured to be

$$A_{FB}^c = 0.052 \pm 0.028 \,(\text{stat.}) \pm 0.012 \,(\text{sys.}).$$

The energy dependence of the asymmetry has been investigated at energies close to the Z^0 peak. Consistency with the predictions of the Standard Model is found.

Combining these measurements with the determination of the asymmetries from semileptonic decays, the following results for b and c quarks are found:

$$A_{FB}^c = 0.032 \pm 0.021 \,(\text{stat.}) \pm 0.015 \,(\text{sys.}),$$

$$A_{FB}^b = 0.096 \pm 0.017 \,(\text{stat.}) \pm 0.008 \,(\text{sys.}),$$

with a correlation coefficient of $+0.15$.

1 Introduction

Within the Standard Model [1], the electroweak interaction has both vector and axial-vector couplings. This

[a] Also at TRIUMF, Vancouver, Canada V6T 2A3
[b] Now at MPI, München, Germany
[c] Also at Shinshu University, Matsumoto 390, Japan
[d] Permanent address: Physics Department, Tufts University, Medford MA 02155, USA

results in a forward-backward asymmetry, A_{FB}, in the differential cross section, $d\sigma/d\cos(\theta)$, for the process $e^+e^+ \to f\bar{f}$, where θ is the angle between the directions of the incoming electron and the outgoing fermion, f. At the Born level and for a centre of mass energy $\sqrt{s} = M_{Z^0}$ this asymmetry depends almost exclusively on the weak coupling constants, v and a, of the fermions involved:

$$A_{FB}^f \approx \frac{3}{4} \frac{2v_e a_e}{4(v_e^2 + a_e^2)} \frac{2v_f a_f}{(v_f^2 + a_f^2)}. \tag{1}$$

For centre of mass energies near the Z^0 peak the interference between the weak and the electromagnetic interactions results in a steep rise of the asymmetry with energy. A measurement of the asymmetry for different fermion species and its energy dependence can therefore be directly related to the couplings in the Standard Model.

In this paper, measurements of the asymmetry of the processes $e^+e^+ \to b\bar{b}$ and $e^+e^+ \to c\bar{c}$ are described. Charged D^* mesons[*] are used to tag $c\bar{c}$ and $b\bar{b}$ events. The charge of the D^* meson is closely correlated to the charge of the primary quark. The D^* momentum is used to separate $b\bar{b}$ from $c\bar{c}$ events. The direction of the primary quark is estimated from the thrust axis of the event. D^* mesons are reconstructed in the decay $D^* \to D^0\pi$, followed by a D^0 decay in the modes $D^0 \to K\pi$, $D^0 \to K\pi\pi^0$ or $D^0 \to K\pi\pi\pi$. The size of the D^* sample is significantly increased by including partially reconstructed D^0 mesons. Compared to asymmetry measurements with a lepton tag at LEP [2,3], the D^* tag provides a much purer sample of primary charm quarks.

[*] Throughout this note D^* always refers to the charged $D^{*\pm}$. Charge conjugate modes are always implied

After a short recapitulation of the basic technique for identifying D^* mesons [4] and a determination of the fragmentation parameters of the process $c \to D^*$, the forward-backward asymmetry of the process $e^+ e^+ \to c\bar{c}$ is extracted from a fit to the charge-weighted thrust distribution of events containing a D^* meson. The energy dependence of this asymmetry is investigated for energies ranging from $M_{Z^0} - 3$ GeV to $M_{Z^0} + 3$ GeV. In a second step, the analysis is extended to measure the asymmetry in the process $e^+ e^- \to b\bar{b}$. Finally the results are combined with those obtained in [2] from an analysis of semileptonic b and c quark decays.

2 The OPAL detector and event selection

Details of the OPAL detector and its performance are described elsewhere [5]. This analysis relies primarily on three of its tracking devices, the vertex chamber, the jet chamber and the z-chambers. Of foremost importance for the precise measurement of invariant masses is the ability of the detector to measure correctly the momentum of tracks and the opening angle between pairs of tracks. The average momentum resolution in $r - \phi$ for the data used in this analysis is found to be $\sigma_{p_t}/p_t = \sqrt{0.020^2 + (0.0015 \cdot p_t/(\text{Gev}/\text{c}))^2}$, where p_t is the momentum transverse to the beam direction. The z-chambers together with the inner tracking chambers yield a polar angle measurement in the barrel region for $|\cos \theta| < 0.72$ (θ being the polar angle) with an angular resolution of 1.7 mrad. In the endcap region, $|\cos \theta| > 0.72$, outside the z-chamber acceptance, an endpoint method is used to improve the track measurement. When a track leaves the detector through the endcap, before reaching the outermost wire of the jet-chamber, the position of the last wire passed, together with the known position of the end plane, gives a polar angle resolution of about 3 mrad [6].

To improve the polar angle resolution further, all tracks in an event are constrained to originate from a common vertex in $s - z$, s being the arc length along the track projected into the $r - \phi$ plane. This vertex is determined with a precision of about 500 μm in z by a running average using tracks from several events. Using only tracks with either z-chamber or endpoint information and constraining them to the event vertex in $s - z$, a polar angle resolution of better than 1 mrad in the barrel region and 2.7 mrad in the endcap region is achieved.

Multihadronic decays of the Z^0 are selected by placing requirements on the number of charged tracks and the amount of energy deposited in the calorimeter, as described in [7]. After requiring that the detector was functioning properly in the periods under investigation a total of 1 254 353 events are selected between 1990 and 1992.

3 Selection of D^* candidates

The D^* mesons are identified via their decay $D^{*+} \to D^0 \pi^+$ followed by one of the following D^0 decays:

i) $D^0 \to K^- \pi^+$ "3-prong"
ii) $D^0 \to K^- \pi^+ \pi^0$ "satellite" (where the π^0 is not reconstructed)
iii) $D^0 \to K^- \pi^+ \pi^- \pi^+$ "5-prong".

Tracks forming a D^* candidate are required to be in the same hemisphere with respect to the thrust axis. The thrust here is calculated from charged tracks and unassociated neutral clusters. Two out of the three tracks forming a D^* candidate in the 3-prong and the satellite channels, and all tracks in the 5-prong channel are required to have either a z-chamber match or an endpoint measurement. In addition tracks have to pass the following quality cuts:

- $|d_0| < 5$ mm, where d_0 is the distance of closest approach between the track and the event vertex in the $r - \phi$ plane;
- $|z_0| < 20$ cm, with z_0 being the distance of closest approach between the track and the event vertex in the z-coordinate;
- $p_t > 250$ MeV/c;
- more than 40 hits in the jet chamber.

For all three channels the selection of D^* candidates is performed in a very similar way. A number of tracks corresponding to the charged multiplicity in the selected D^0 decay are combined, with the assumption that one is a kaon and the others are pions. The total charge of the tracks has to add up to zero. The invariant mass, $M_{D^0}^{\text{cand}}$, of this combination is calculated. If it lies within a specified window, the combination is retained as a D^0 candidate. Another track, the slow pion, with pion mass assumed and a charge opposite to the charge of the kaon candidate track, is combined with the D^0 candidate, and its mass is calculated. The combination is considered a D^* candidate if the mass difference between this mass and the D^0 candidate mass is within certain limits.

The $M_{D^0}^{\text{cand}}$ mass window used for the 3-prong and 5-prong samples is:

- $1790 \text{ MeV/c}^2 < M_{D^0}^{\text{cand}} < 1940 \text{ MeV/c}^2$.

For the satellite channel the π^0 is not reconstructed and therefore is not included in the invariant mass calculation which yields a second peak in the $M_{D^0}^{\text{cand}}$ distribution around $M_{D^0}^{\text{cand}} \approx 1600 \text{ MeV/c}^2$ (Fig. 1). A number of different decay modes contribute to this channel, with the dominant mode being $D^0 \to K^- \rho^+$ with $\rho^+ \to \pi^+ \pi^0$. The width of this peak is about twice as large as that in the 3-prong channel. Candidates in this satellite channel are selected by requiring

- $1410 \text{ MeV/c} < M_{D^0}^{\text{cand}} < 1770 \text{ MeV/c}^2$.

At low values of $x_{D^*} = 2 \cdot E_{D^*}/E_{\text{cms}}$, where E_{D^*} is the energy of the D^* meson, and E_{cms} the centre of mass energy, the combinatorial background becomes increasingly important. To enhance the signal to background ratio, only D^* candidates with $x_{D^*} > 0.2$ are used for 3-prong and satellite decays, while $x_{D^*} > 0.5$ is required of 5-prong candidates. A further large suppression of the background is achieved by exploiting the isotropic decay distribution of the D^0 in its rest frame. The distribution
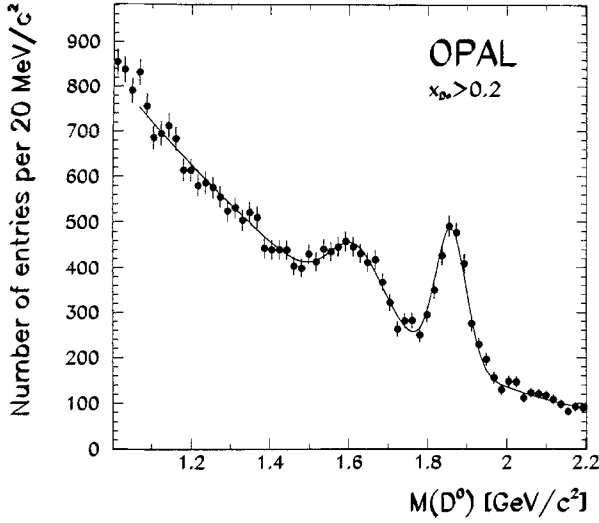
Fig. 1. Spectrum of the invariant $K\pi$ mass, $M_{D^0}^{cand}$. Clearly seen is the satellite enhancement below the nominal M_{D^0} mass mostly due to the decay $D^0 \to \rho^+ K^-$, and the subsequent decay $\rho^+ \to \pi^+ \pi^0$. No attempt has been made to reconstruct the π^0. It should be noted that not all of the candidates referred to as satellite candidates in the text are visible on this plot. For a detailed discussion see Sect. 3

Fig. 2a–c. Spectrum of $M_{D^*}^{cand} - M_{D^0}^{cand}$ a for the 3-prong for $x_{D^*} > 0.2$, b the satellite for $x_{D^*} > 0.2$ and c the 5-prong decay for $x_{D^*} > 0.5$. The histograms show the signal sample, the points the background distributions obtained with the slow pion reflection method as described in the text. The broadening of the peak due to partially reconstructed D^0 mesons is clearly seen in the satellite and in the 5-prong sample. The solid line in c indicates the spectrum for background plus partially reconstructed D^0 decays, as predicted by the Monte Carlo. This class of candidates is absent in the 3-prong sample

of $\cos(\theta^*)$, where θ^* is the angle between the direction of the K in the rest frame of the D^0 candidate and the direction of the D^0 candidate in the laboratory frame, is expected to be flat for a D^0 decay. Background events show pronounced peaks at $\cos(\theta^*) = \pm 1$. Events are selected if

- $|\cos(\theta^*)| < 0.8$ for the 3-prong and satellite channel for $0.2 < x_{D^*} < 0.5$;
- $|\cos(\theta^*)| < 0.9$ for the 3-prong and satellite channel for $x_{D^*} > 0.5$;
- $\cos(\theta^*) > -0.9$ for the 5-prong channel.

In the 5-prong sample it frequently arises that several candidates per event pass the above cuts. To avoid double counting of events and, at the same time, to further reduce the background, only the D^* candidate whose reconstructed $M_{D^0}^{cand}$ is closest to the true D^0 mass of 1.8645 GeV is retained. It has been checked using wrong-charge background combinations that this method does not produce any biases in the $\Delta M = M_{D^*}^{cand} - M_{D^0}^{cand}$ distribution. In particular no spurious peak around $\Delta M = 145 \text{ MeV}/c^2$ has been observed, which would influence the background determination described below.

The value of ΔM is required to lie in the range

- $142 \text{ MeV}/c^2 < \Delta M < 149 \text{ MeV}/c^2$ for the 3-prong and the 5-prong decay,
- $141 \text{ MeV}/c^2 < \Delta M < 151 \text{ MeV}/c^2$ for the satellite sample.

The ΔM spectra are shown in Fig. 2.

Additional complications arise in the case of the satellite and the 5-prong channels. Both samples contain a significant number of candidates where the decay of the D^0 is only partially reconstructed. Either some decay products are missed completely, as is the case with the

π^0 in the satellite channel or for other higher multiplicity decay modes of the D^0, or wrong tracks are combined with correct ones and the candidate passes the selection cuts. A significant fraction of this class of events is still associated with the correct slow pion candidate track. These events have to be considered signal for the asymmetry measurement, because the charge correlation between the slow pion and the D^* remains intact. They are responsible for a broad peak in the ΔM spectrum shown in Fig. 2c. This enhancement means it is still possible to count the number of such events, as described in the following section. For partially reconstructed D^0 candidates with a wrongly associated slow pion candidate track, the charge correlation between the D^* and the slow pion is broken and, in addition, no enhancement is present in the ΔM spectrum. These events are correctly accounted for as background events.

In the subsequent analysis the scaled energy, x_{D^*}, is used to separate the contributions from $b\bar{b}$ and $c\bar{c}$ events to the observed asymmetry of events containing a D^*. If the D^0 is not fully reconstructed, the x_{D^*} calculated from the sum of the candidate tracks is not correct. For the signal events, however, the slow pion is identified cor-

rectly and the information from the slow pion candidate can be used to estimate x_{D^*}. Its momentum in the laboratory frame carries most of the information about the D^* momentum itself. Assuming that the slow pion is produced at rest, its momentum is related to the D^* momentum by $p_{D^*} = p_{\pi,s} \cdot M_{D^*}/m_\pi$. Taking the small momentum of the π in the D^* rest frame into account this equation is modified to:

$$p_{D^*} = p_{\|\pi} \cdot \frac{M_{D^*}}{\sqrt{(m_\pi^2 + (p_\pi^R)^2)} + p_{\|\pi}^R/\beta} \quad . \tag{2}$$

Here the subscript π refers to the slow pion, the superscript R to momenta in the D^* rest frame, β to the velocity of the D^*, and the subscript $\|$ to the momentum component parallel to the D^* direction. Since the latter is not correctly known in partially reconstructed decays, (2) can be only approximately evaluated. Setting $p_{\|\pi} = p_\pi$ and $\beta = 1$ introduces a very small error. More substantial uncertainties are caused by estimating $p_{\|\pi}^R$, which can vary between -40 MeV/c and $+40$ MeV/c. Setting it to zero introduces an error with a roughly rectangular distribution of the approximate $\tilde{x}_{D^*}$ around the true x_{D^*} value with a variance of 16%. To evaluate the reliability of this method and to obtain its resolution function, $E(x_{D^*}, \tilde{x}_{D^*})$, it has been applied to fully reconstructed 3-prong candidates. The correct x_{D^*} value obtained from the sum of the momenta of the three tracks was compared with the $\tilde{x}_{D^*}$ obtained with the approximate method outlined above. No systematic shifts were observed.

4 Determination of the background

The dominant source of background to the D^* signal is random combinations of tracks satisfying the mass cuts on M_{D^0} and ΔM. The background shape is determined using a hemisphere mixing technique. A $K\pi$ candidate is selected using the same cuts as before with the exception that two charge combinations are allowed. The charges of the candidate tracks have to add up to zero or to ± 2, with the additional constraint that the total charge of all pion candidates has to be ± 1. To complete the background combination the slow π candidate track is taken from the opposite hemisphere. Its charge is chosen such

that the total charge of the combination is ± 1. This track is reflected about the origin to bring it into the same hemisphere as the D^0 candidate, and the invariant mass of this combination is calculated. This hemisphere mixing method ensures that the background sample is free of the correlations between the slow pion and the D^0 tracks which lead to the peak in the ΔM spectrum. The background sample is normalized to yield the same number of candidates as the signal sample for 180 MeV/c^2 < ΔM < 200 MeV/c^2.

In Fig. 2a–c the signal and background distributions are shown for the three decay channels investigated. Whereas there is a clear peak for the 3-prong decay (a), both the satellite and the 5-prong decays exhibit broad shoulders around the expected ΔM for the signal. This broadening is due to the inclusion of partially reconstructed D^0 decays. This is most clearly seen in Fig. 2c. Here the Monte Carlo prediction of the expected enhancement from partially reconstructed decays over the background is shown for comparison. The broad peak underneath the narrow ΔM peak expected from fully reconstructed D^* decays is well described in the Monte Carlo. Furthermore detailed Monte Carlo studies show that the distribution and the rate of the background in the signal region is accurately described by this method of using a reflected slow pion.

In the 3-prong and satellite samples, the number of background events under the signal is determined by a fit of a function $a \cdot (\Delta M - M_\pi)^b$ to the ΔM distribution of the background sample with a and b as free parameters in the fit, and by integrating this function over the ΔM range selected. In the 5-prong sample, this function does not describe the shape of the background. The number of background events is determined by simply counting the number of candidates in the normalized background distribution for the selected ΔM range. The number of D^* mesons is found by subtracting the number of background events from the total number of candidates.

In Table 1 the numbers of events are listed as a function of x_{D^*}. The numbers of signal and background events are shown, determined for candidates selected in all three decay modes, integrated over all centre of mass energy points around M_Z. In total 6507 ± 147 D^* mesons are identified. Of these 538 ± 39 are collected at energies off the peak of the Z^0 resonance.

Table 1. Numbers of D^* mesons in the three channels $D^* \rightarrow (K\pi)\pi$, $D^* \rightarrow (K\pi\pi^0)\pi$ and $D^* \rightarrow (K\pi\pi\pi)\pi$ for all centre of mass energies. The background error includes the uncertainty in the extrapolation of the background under the signal peak and systematic effects. The error on $N_{D^*}^{obs}$ is $(\Delta N_{D^*}^{obs})^2 = N_{D^*}^{obs} + N_{bck}^{obs} + \Delta N_{bck}^{obs2}$

x_{D^*}	$D^* \rightarrow (K\pi)\pi$		$D^* \rightarrow (K\pi\pi^0)\pi$		$D^* \rightarrow (K\pi\pi\pi)\pi$	
	$N_{D^*}^{obs}$	N_{bck}^{obs}	$N_{D^*}^{obs}$	N_{bck}^{obs}	$N_{D^*}^{obs}$	N_{bck}^{obs}
0.2–0.3	405 ± 39	727 ± 20	1202 ± 87	3516 ± 53	–	–
0.3–0.4	303 ± 27	290 ± 11	897 ± 58	1363 ± 33	–	–
0.4–0.5	281 ± 21	116 ± 8	661 ± 41	544 ± 21	–	–
0.5–0.6	308 ± 21	73 ± 7	660 ± 42	616 ± 22	398 ± 42	655 ± 26
0.6–0.7	197 ± 16	30 ± 4	416 ± 28	212 ± 13	230 ± 25	202 ± 14
0.7–0.8	124 ± 12	11 ± 3	130 ± 15	62 ± 7	134 ± 15	44 ± 6
0.8–1.0	56 ± 8	5 ± 2	41 ± 10	30 ± 4	64 ± 10	18 ± 4
$\sum$	1674 ± 60	1252 ± 26	4007 ± 124	6343 ± 71	826 ± 52	919 ± 30

5 Measurement of the $c \rightarrow D^*$ fragmentation function

In order to separate the contributions to the D^* asymmetry from charm and bottom quarks, the D^* fragmentation parameters must be known. The measurement presented in [4] is extended to include all data collected between 1990 and 1992, at all centre of mass energies. Since an accurate efficiency and x_{D^*} determination is necessary, only D^* candidates found in the 3-prong channel are used in this part of the analysis. The requirements on the signal to noise ratio are more stringent than in the asymmetry measurement. Therefore, in addition to the cuts presented in Sect. 3, the particle identification power of the OPAL detector is used to help in identifying the kaon [8]. For $x_{D^*} < 0.5$ the measured rate of energy loss in the jet chamber, dE/dx, of a kaon candidate track has to agree with the value expected for a kaon with a probability of more than 0.1.

D^* mesons produced in Z^0 decays originate primarily from $c\bar{c}$ and $b\bar{b}$ events. Some contribution is expected from gluon splitting, $g \rightarrow c\bar{c}$, occurring mostly at low x_{D^*}. However, because of the large gluon mass required, these contributions should be very small. The JETSET model [9] indicates that less than 1% of D^* mesons with $x_{D^*} > 0.2$ originate from this source. Therefore this source will be neglected.

The c quark fragmentation parameters are determined by a fit to the x_{D^*} distribution of 2660 3-prong candidates satisfying the dE/dx requirements described above, of which 1608 ± 58 are signal, using an unbinned generalized maximum-likelihood fit [11]. The likelihood function is defined as

$$\log \mathscr{L} = \log \frac{N^n e^{-N}}{n!}$$
$$+ \sum_{i=1}^{n} \log\{(2 \cdot [F_b \cdot P_b(D^* \rightarrow \pi K\pi) \cdot d'_{b \rightarrow D^*}(x_i)$$
$$+ F_c \cdot P_c(D^* \rightarrow \pi K\pi) \cdot d_{c \rightarrow D^*}(x_i)] + b(x_i))\}, \quad (3)$$

where the sum goes over all candidate events, and

● N is the total number of candidates expected and depends on the current set of parameters, and n is the number of candidates actually observed. The first term in the likelihood function, the Poisson term, is included to increase the sensitivity of the fit to the rate.
● F_q is the ratio of the partial width, $\Gamma_{Z^0 \rightarrow q\bar{q}}$, to the total hadronic width, $\Gamma_{Z^0 \rightarrow \text{hadron}}$, of the Z^0;
● $P_q(D^* \rightarrow \pi K\pi)$ is the product branching ratio for a D^* meson to be produced from a quark q and to decay into the channel $D^* \rightarrow D^0\pi \rightarrow \pi K\pi$, $P_q(D^* \rightarrow \pi K\pi) =$ BR $(q \rightarrow D^*X) \cdot$ BR $(D^* \rightarrow D^0\pi) \cdot$ BR $(D^0 \rightarrow K\pi)$.
● $d'_{b \rightarrow D^*}(x_{D^*})$ is a function describing the shape of the $x_{b \rightarrow D^*}$ distribution. An empirical parametrization is used [4], with

$$d'_{b \rightarrow D^*}(x_{D^*}) = A \cdot \exp\left(\frac{-(x_{D^*} - B)^2}{C}\right)$$
$$\cdot \left(1 + \frac{D}{x_{D^*}} + E \cdot x_{D^*}^2 + F \cdot x_{D^*}^3\right), \quad (4)$$

and the parameters A to F determined from Monte Carlo and other experiments as described below;
● The $x_{c \rightarrow D^*}$ distribution is parametrized with a function of the Peterson shape [10]:

$$d_{c \rightarrow D^*}(x_{D^*}) \propto \left(x_{D^*} \cdot \left[1 - \frac{1}{x_{D^*}} - \frac{\epsilon_{D^*}}{1 - x_{D^*}}\right]^2\right)^{-1}; \quad (5)$$

● $b(x_{D^*})$ is the background as a function of x_{D^*}. The function is determined by fitting the observed number of background events with a function $\alpha \cdot \exp(-\beta x_{D^*})$, with α and β free parameters, separately for $x_{D^*} < 0.5$ and $x_{D^*} > 0.5$, and then dividing this function by the efficiency $\varepsilon_{3\text{pr}}$ for identifying a D^* meson.

In this fit, the two parameters $F_c \cdot P_c(D^* \rightarrow \pi K\pi)$ and ϵ_{D^*} are allowed to vary freely. For the final result, the fragmentation parameter ϵ_{D^*} is translated into $\langle x_{c \rightarrow D^*} \rangle$.

The contribution from b quarks to the x_{D^*} distribution is kept fixed in the fit. The fragmentation of b-quarks is assumed to be described by the Peterson form [10] with $\epsilon_b = 0.0055 \pm 0.0018$, as measured from the spectra of leptons in b-decays at LEP [12]. The JETSET Monte Carlo model [9] is used to calculate the resulting shape of the D^* momentum spectrum. The rate of D^* production from b-hadron decay is determined from lower energy measurements [13, 14] and some simple modelling of the B_s contribution [4] (see below). Together with the recent OPAL measurement of $F_b = 0.221 \pm 0.008$ (stat. + sys.) [15] a value $F_b \cdot P_b(D^* \rightarrow \pi K\pi) = (1.17 \pm 0.16) \cdot 10^{-3}$ is found.

In Table 2 the systematic errors pertinent to the fragmentation fit are listed. The error in the background determination has been estimated by comparing different methods of measuring the background as described in [4]. Uncertainties due to detector effects and selection criteria are included in this error. The efficiency for reconstructing a D^* has been calculated using Monte Carlo events which were passed through a complete simulation of the OPAL detector [9, 16, 17]. About 52 000 fully simulated D^* 3-prong decays were used. No significant variation in the efficiency with x_{D^*} below and above 0.5

Table 2. Changes in the fit results due to variations in the efficiency and background (above) and the contribution from b quarks (below)

Error source	$\Delta(F_c \cdot P_c(D^* \rightarrow \pi K\pi))$	$\Delta(\langle x_{D^*} \rangle)$
Systematic error specific to the fragmentation function fit		
Background	$0.07 \cdot 10^{-3}$	0.010
Efficiency	$0.05 \cdot 10^{-3}$	0.004
Final error assigned	$0.09 \cdot 10^{-3}$	0.011
Systematic error from $b \rightarrow D^*$		
ε_b	$0.04 \cdot 10^{-3}$	0.002
$F_b \cdot P_b(D^* \rightarrow \pi K\pi)$	$0.12 \cdot 10^{-3}$	0.008
$\Upsilon(4S)$ shape	$0.02 \cdot 10^{-3}$	0.009
Final error assigned	$0.13 \cdot 10^{-3}$	0.013
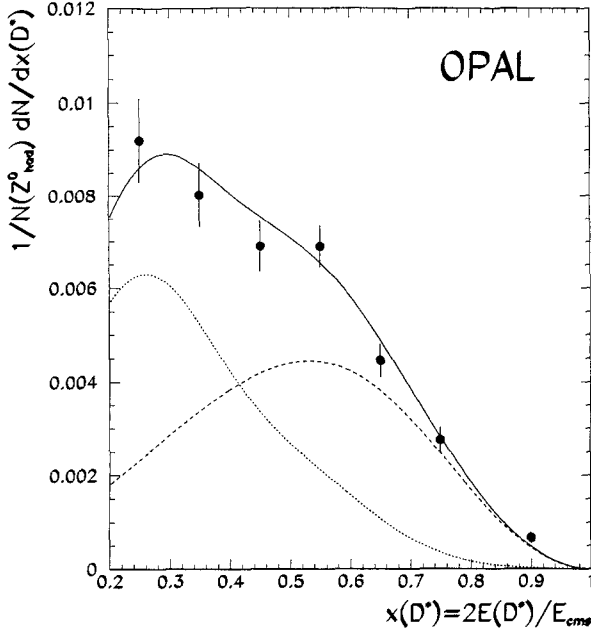
Fig. 3. Observed yield of D^* mesons normalized to the total number of multihadronic events, as a function of x_{D^*}. The solid line is the result of the unbinned log-likelihood fit. The dashed line shows the $c\bar{c}$, the dotted the $b\bar{b}$ contribution. The errors shown are statistical only

was observed. For $x_{D^*} < 0.5$ the efficiency is $\varepsilon_{3\mathrm{pr}} = 0.302 \pm 0.003$, and for $x_{D^*} > 0.5$ $\varepsilon_{3\mathrm{pr}} = 0.338 \pm 0.004$. The increase is due to the loosening of the cuts on $\cos(\theta^*)$ and dE/dx for the kaon candidate track when $x_{D^*} > 0.5$. An overall relative error of 3% has been assigned to the efficiency to allow for possible misrepresentations of the data by the Monte Carlo simulation.

The influence of the fixed b-fragmentation function on the results has been investigated by varying the input parameters within their errors. The modelling of the decay of B mesons into D^* mesons has been checked by boosting the $x_{b \to D^*}$ distribution into the b rest frame and comparing its shape with measurements at the $\Upsilon(4S)$ [18, 19]. Good agreement with the data is found. The error assigned to this source corresponds to the statistical error of this comparison.

The observed yield of D^* mesons as a function of x_{D^*} corrected for efficiency together with the fit results is shown in Fig. 3. The final results, including all systematic errors, are

$$F_c \cdot P_c (D^* \to \pi K \pi) = (1.17 \pm 0.07 \pm 0.09 \pm 0.13) \cdot 10^{-3},$$

$$\langle x_{c \to D^*} \rangle = 0.496 \pm 0.011 \pm 0.011 \pm 0.013,$$

where the errors quoted are the statistical error, the systematic error specific to this analysis and the systematic error due to external sources, mainly the contribution from b-decays.

6 Measurement of the asymmetry

The forward-backward asymmetry is defined as

$$A_{FB} = \frac{\int_0^1 \frac{d\sigma}{dy} \, dy - \int_{-1}^0 \frac{d\sigma}{dy} \, dy}{\int_0^1 \frac{d\sigma}{dy} \, dy + \int_{-1}^0 \frac{d\sigma}{dy} \, dy}, \tag{6}$$

where y is the cosine of the polar angle of the outgoing fermion with respect to the incoming fermion. In events containing a D^*, the direction y is well described by $y = q \cdot \cos(\theta_{\mathrm{thrust}})$, where q is the charge of the D^* and θ_{thrust} is the angle of the thrust axis with respect to the beam. The sign of the thrust axis is chosen such that the scalar product of the thrust axis with the D^* direction is positive. In the Born approximation the differential cross section for the reaction $e^+ e^+ \to q\bar{q}$ is proportional to [1]

$$\frac{d\sigma}{dy} \propto 1 + y^2 + \tfrac{8}{3} A_{FB}^q \cdot y. \tag{7}$$

Higher order electroweak and strong corrections can in principle change this shape. Their effect however is expected to be very small.

An unbinned maximum likelihood fit [11] is used to extract the asymmetries. The likelihood function has the general form

$$\log \mathscr{L} = \sum_{i=1}^n \log (P \cdot \alpha \, (y_i) \cdot (1 + y_i^2 + \tfrac{8}{3} A_{FB}^q \cdot y_i)). \tag{8}$$

Here P is a normalization factor, and $\alpha\,(y)$ the acceptance as a function of y. The parameter to be determined in the fit is A_{FB}^q. The acceptance is assumed to be independent of the D^* charge, and is therefore an even function of y. The only A_{FB}^q dependent term is an odd function of y. As a result, the normalization and acceptance are both independent of A_{FB}^q leading to a constant term in the sum over all candidates, which does not influence the maximization. The consequences of this assumption will be discussed further in the next section on the determination of the systematic errors.

The explicit form of the likelihood function used for maximization is

$$\log \mathscr{L} = \log \mathscr{L}_{3\mathrm{pr}} + \log \mathscr{L}_{\mathrm{sat}} + \log \mathscr{L}_{5\mathrm{pr}}. \tag{9}$$

Each of the terms has the form

$$\log \mathscr{L} = \sum_{i=1}^n \log \{ P_b (x_{D^*i}) \cdot (1 + y_i^2 + \tfrac{8}{3} A_{FB}^{D^*,b} \cdot y_i)$$

$$+ (P_c (x_{D^*i}) \cdot (1 + y_i^2 + \tfrac{8}{3} A_{FB}^{D^*,c} \cdot y_i)$$

$$+ P_{\mathrm{bck}} (x_{D^*i}) \cdot (1 + y_i^2) \}, \tag{10}$$

where the sum goes over all n D^* candidate events, $A_{FB}^{D^*,b}$ and $A_{FB}^{D^*,c}$ are the asymmetries seen in the D^* tagged $b\bar{b}$ and $c\bar{c}$ events respectively. The background is assumed to have no asymmetry. Events with more than one D^* candidate are only counted once. If within one

event candidates are found in more than one channel, a 3-prong candidate is chosen over a satellite candidate, which in turn is preferred over a 5-prong candidate. In the 3-prong decay P_b, P_c, P_{bck} are defined as

$$P_b(x_{D*}) = \frac{N_D^{obs}(x_{D*})}{N^{tot}(x_{D*})}$$

$$\cdot \frac{f_{b\to D*}(x_{D*})}{f_{b\to D*}(x_{D*}) + f_{c\to D*}(x_{D*})},$$

$$P_c(x_{D*}) = \frac{N_D^{obs}(x_{D*})}{N^{tot}(x_{D*})}$$

$$\cdot \frac{f_{c\to D*}(x_{D*})}{f_{b\to D*}(x_{D*}) + f_{c\to D*}(x_{D*})}, \quad (11)$$

$$P_{bck}(x_{D*}) = \frac{N_{bck}^{obs}(x_{D*})}{N^{tot}(x_{D*})},$$

where N_{D*}^{obs} are the observed number of $D*$ mesons, N_{bck}^{obs} the observed number of background events, both as given in Table 1, and $N^{tot} = N_{D*}^{obs} + N_{bck}^{obs}$. The functions f are defined in terms of the functions introduced in Sect. 5: $f_{q\to D*}(x_{D*}) = F_q P_q(D*\to\pi K\pi) d_{q\to D*}(x_{D*})$. In the satellite and 5-prong channels the $f_{q\to D*}(x_{D*})$ are replaced by a folding integral

$$\tilde{f}(\tilde{x}_{D*}) = \int f(x_{D*}) E(x_{D*}, \tilde{x}_{D*}) dx_{D*}, \quad (12)$$

since $\tilde{x}_{D*}$ is determined using the approximation described in Sect. 3. The function $E(x_{D*}, \tilde{x}_{D*})$ describes the resolution function for this method, accounting for the additional smearing introduced.

Two separate measurements are made, a one parameter fit to determine A_{FB}^c, and a two parameter fit to measure both A_{FB}^c and A_{FB}^b.

For the one parameter fit A_{FB}^b is taken from the measurement using semileptonic b-decays [2]. This asymmetry, $A_{FB}^{b,mix} = (0.0701 \pm 0.0827 \cdot A_{FB}^c)$ is first corrected for the effective mixing at LEP with $\chi_{eff}^l = 0.119 \pm 0.012$ [20] to obtain A_{FB}^b. Then the effective $D*$ asymmetry is calculated correcting for the mixing in the neutral B mesons,

$$A_{FB}^{D*,b} = A_{FB}^b \left[\frac{1}{BR(b\to D^{*\pm}X)} \right.$$

$$\cdot \{ p_u \cdot BR(B_u \to D^{*\pm}X)$$

$$+ p_d \cdot BR(B_d \to D^{*\pm}X) \cdot (1 - 2\chi_d)$$

$$\left. + p_s \cdot BR(B_s \to D^{*\pm}X) \cdot (1 - 2\chi_s) \} \right]$$

$$\cdot (1 - 2\zeta_{D*}). \quad (13)$$

The p_q are the relative fractions to pull a quark of flavour q from the sea. The values used are $p_u = p_d = 0.40 \pm 0.05$, $p_s = 0.13 \pm 0.05$ [21]. The χ_s, χ_d give the mixing probability for strange and down type B mesons, respectively. Other processes resulting in $D*$ mesons with the wrong sign have been allowed for by including the term $(1 - 2\zeta_{D*})$.

The values for the branching ratios BR $(B_{u,d}\to D^{*\pm}X)$ and BR $(B_s\to D^{*\pm}X)$ used in [4] have been updated to reflect some recently published measurements, BR $(B_{u,d}\to D^{*\pm}X) = 0.269 \pm 0.035$ [13]. The B_u and B_d mesons are assumed to be produced in equal numbers. The, as yet unmeasured, branching ratio BR $(B_s\to D^{*\pm}X)$ has been estimated as in [4] to be BR $(B_s\to D^{*\pm}X) = 0.095 \pm 0.046$. Furthermore it is assumed that BR $(B_s\to D^{*\pm}X) = BR(B_u\to D^{*\pm}X)$, which is justfied from Monte Carlo modeling. The mixing parameter in the B_d system has been measured by ARGUS and CLEO to be $\chi_d = 0.161 \pm 0.026$ [22, 23]. For this value of χ_d the average $B\bar{B}$ mixing measurement by OPAL [12] is compatible with the theoretical expectation of almost maximal mixing. In this analysis a value of $\chi_s = 0.5$ is assumed and allowed to vary from $\chi_s = 0.24$ to $\chi_s = 0.5$. Another process contributing $D*$ mesons with the "wrong" signs is the decay $b\to cW$, $W\to\bar{c}s$, with the $D*$ formed from the $\bar{c}$. Its branching ratio BR $(B\to D^{*-}X)$ is expected to be at most 1% [24]. Therefore a value $\zeta_{D*} = 0.025 \pm 0.025$ is assumed. The final value used for $A_{FB}^{b,D*}$ in the one parameter fit is $A_{FB}^{b,D*} = 0.064 \pm 0.015$.
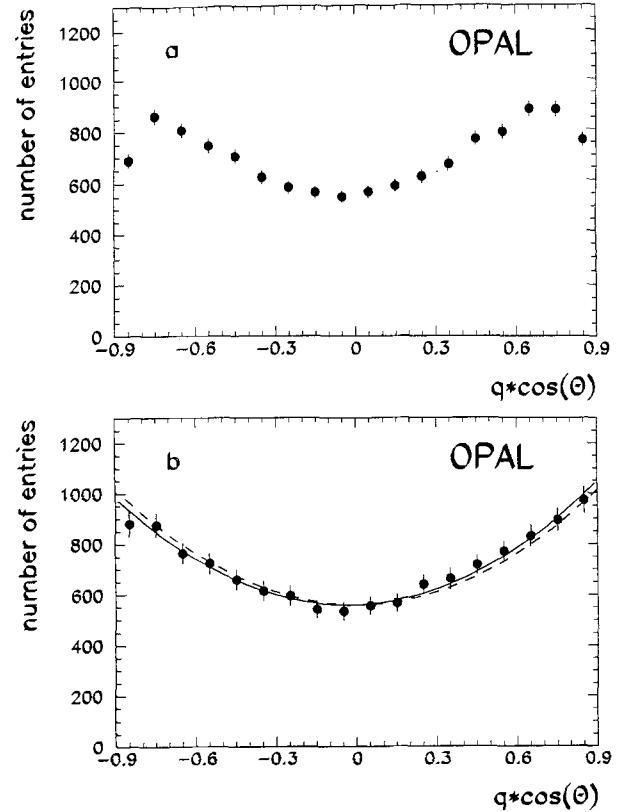
Fig. 4a, b. a The $q\cdot\cos(\theta_{thrust})$ distribution of all $D*$ candidates events found on the peak of the Z^0 resonance. **b** The $q\cdot\cos(\theta_{thrust})$ distribution for all peak candidate events (points) after correcting for the acceptance. The errors on the points include the errors due to this correction. As discussed in the text, the acceptance is not used in the maximum likelihood fit, and has been introduced for demonstration purposes only. Superimposed are the result of the maximum likelihood fit (solid line) and the expectation for no asymmetry in $D*$ tagged events (dashed line)

The $q \cdot \cos(\theta_{\text{thrust}})$ distribution for all candidates is shown in Fig. 4. In this figure, an acceptance correction derived from Monte Carlo has been applied to allow for a better comparison between the $q \cdot \cos(\theta_{\text{thrust}})$ distribution of the data and the fit result. It should be noted that this aceptance is not used in the fit.

The sample collected on the peak of the Z^0 resonance has been fitted to extract A_{FB}^c. The result of the one parameter fit is

$$A_{FB}^c = 0.052 \pm 0.028 \,(\text{stat.}) \quad \text{for} \quad x_{D*} > 0.2 \,.$$

The c-purity of the signal in this sample is 55%. Restricting x_{D*} to be larger than 0.5 the c-purity is increased to 73%. The fit then yields $A_{FB}^c = 0.039 \pm 0.034\,(\text{stat.})$. Fitting for A_{FB}^c and A_{FB}^b simultaneously yields

$$A_{FB}^c = 0.038 \pm 0.044 \,(\text{stat.}),$$

$$A_{FB}^b = 0.139 \pm 0.097 \,(\text{stat.}) \quad \text{for} \quad x_{D*} > 0.2 \,,$$

with a statistical correlation coefficient of -0.741. The fits give consistent results. The two parameter fit demonstrates that the $D*$ measurement is considerably more sensitive to the c quark asymmetry than to the b quark asymmetry.

7 Systematic errors

The basic assumption in the maximum likelihood fit is that background and signal can be described by the same symmetric acceptance, α. If this assumption is not true the acceptance has to be introduced explicitly in (10). There are no indications in Monte Carlo studies nor in the data that this assumption is not justified. Taking the worst possible deviation from this assumption compatible with the available Monte Carlo statistics, a change in the asymmetry of less than 0.005 is found. An error of 0.005 is therefore assigned to cover this source.

Another potentially important source of systematic error is a possible asymmetry in the background or a deviation from the assumed $1 + y^2$ form. This has been checked by selecting background $D*$ candidates from a mass band above the ΔM mass window and background candidates found with a reflected slow pion, and investigating their $q \cdot \cos(\theta_{\text{thrust}})$ distribution. No evidence for an asymmetry or a deviation from the assumed form has been found. The background asymmetry is found to be less than 0.005. Assuming a background asymmetry of 0.005 leads to a shift in the c-asymmetry of 0.006, which is assigned as the error due to this source.

The approximate determination of x_{D*} in the satellite and 5-prong channels introduces an additional source of error by smearing the x_{D*} distribution. This has been investigated by repeating the 3-prong analysis with x_{D*} redetermined using only information from the slow pion. This allows a direct comparison between the true x_{D*}, as available in the 3-prong decay, and the corrected x_{D*} used in the other two channels. No significant change in the result has been observed and the deviation compatible with this leads to a systematic error of 0.002.

Table 3. List of the systematic errors contributing to the measured asymmetry of the process $e^+e^- \to c\bar{c}$. In the second column, the errors for the one parameter fit are listed, in the third and fourth the errors from the two parameter fit. Here the signs of the errors indicate the relative direction in which the asymmetries change for the particular systematic error source

Systematic error source	$\Delta(A_{FB}^c)$	$\Delta(A_{FB}^c)$	$\Delta(A_{FB}^b)$
Same acceptance for background and signal	0.005	+0.005	+0.005
Background determination	0.004	+0.007	+0.020
Background asymmetry	0.006	+0.002	+0.029
Detector effects	0.002	+0.002	+0.006
Uncertainty in x_{D*} scale	0.001	+0.002	+0.006
ϵ_b	0.001	+0.001	+0.001
$F_b \cdot P_b$	0.001	+0.001	-0.009
ϵ_c	0.001	+0.001	-0.002
$F_c \cdot P_c$	0.001	+0.001	+0.001
ζ_{D*}	0.002	+0.000	+0.009
$b\bar{b}$ asymmetry	0.006	N/A	N/A
Effective $B\bar{B}$ mixing in $D*$ events	0.005	+0.000	+0.030
Thrust instead of quark direction	0.001	+0.001	+0.001
Total	0.012	0.010	0.049

The error due to the determination of the background has been investigated by varying the background numbers within their errors listed in Table 1. In addition, the background has been redetermined using a counting method for all channels instead of just for the 5-prong channel. The final systematic error assigned due to background determination takes both effects into account.

An important input for the asymmetry calculation is the b to c ratio in the $D*$ spectrum as a function of x_{D*}, as determined in Sect. 5. The systematic errors for this were also discussed in there. Their influence on the final asymmetry has been investigated by varying the different parameters within their errors.

The error in the one parameter fit due to the asymmetry from $b\bar{b}$ events has been estimated in the same manner by varying $A_{FB}^{D*,b}$ within the quoted errors.

As mentioned previously, the thrust axis has been used to estimate the direction of the primary quark. As in [2] an error of 0.001 has been assigned to the asymmetry due to this approximation.

A list of the contributions to the systematic error can be found in Table 3. Also shown are the errors of the two parameter fit with both asymmetries as free parameters. They have been determined in an analogous manner to those for the one parameter fit.

To study the stability of the result a number of consistency checks have been performed. The sample has been subdivided according to the year in which data were taken and the decay channel. The cuts used for identifying $D*$ mesons have been varied around their standard values. All changes observed in the results are compatible with the statistical error.

8 Energy dependence of the asymmetry

To investigate the energy dependence of the asymmetry in the process $e^+e^+ \to c\bar{c}$, the selection of $D*$ candidates

and the fit have been repeated at centre of mass energies below and above M_{Z^0}. Only data from 1990/1991 are available with energies off the Z^0 peak. Below the peak, 489 $D*$ candidate events containing 220 ± 25 signals events are found in the three decay modes investigated at an average centre of mass energy of 89.75 GeV. Above the peak 691 candidate events containing 318 ± 30 signal events are identified at an average centre of mass energy of 92.64 GeV.

Over the range of energies covered, for a Higgs mass of 300 GeV/c² and a top mass of 130 GeV/c², the asymmetry of the process $e^+e^- \to b\bar{b}$ is expected to vary from 0.025 at 88.48 GeV to 0.116 at 93.72 GeV [25]. This predicted energy dependence, together with the measured value of A_{FB}^b at 91.2 GeV, has been used to calculate the energy dependence of the asymmetry of $D*$ mesons from the decay of b quarks.

The results of the fits are:

$$A_{FB}^c = -0.14 \pm 0.14 \, (\text{stat.}),$$

$$88.4 \, \text{GeV} < E_{\text{cms}} < 90.3 \, \text{GeV},$$

$$A_{FB}^c = 0.18 \pm 0.12 \, (\text{stat.}),$$

$$91.9 \, \text{GeV} < E_{\text{cms}} < 93.8 \, \text{GeV}.$$

In Fig. 5 the measured asymmetries are plotted versus the energy. Also shown is the prediction of ZFITTER [25] for a top mass of 130 GeV/c² and a Higgs boson mass
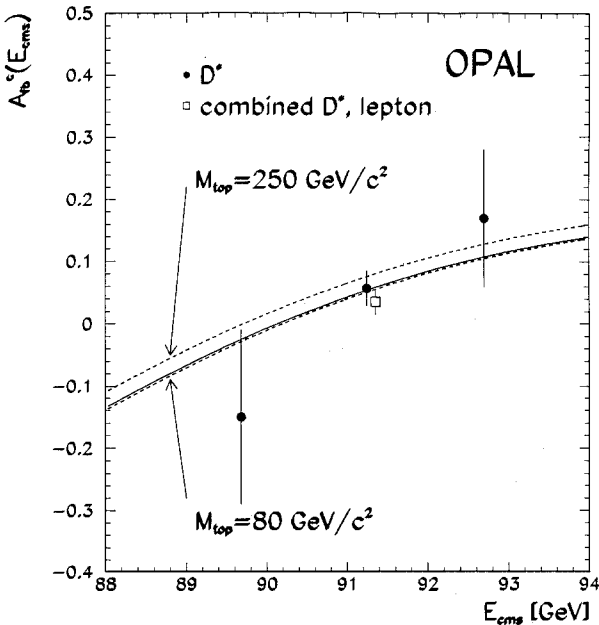
Fig. 5. Forward-backward asymmetry of the process $e^+e^- \to c\bar{c}$ as a function of the centre of mass energy. The closed points are the measured asymmetries from the $D*$ analysis. The open point is the on-peak measurement after combination with the result from the lepton analysis. Errors shown are statistical only. The predictions from ZFITTER for top mass of 130 GeV/c² and a Higgs boson mass of 300 GeV/c² (solid line) are superimposed. The dashed lines indicate the range of A_{FB}^c, when the top mass changes from 80 GeV/c² to 250 GeV/c²

of 300 GeV/c². The dashed lines indicate the range of A_{FB}^c, when the top mass changes from 80 GeV/c² to 250 GeV/c². The same systematic errors as discussed in Sect. 7 apply to these measurements. In addition, the energy dependence of the asymmetry of the process $e^+e^- \to b\bar{b}$ introduces a source of error. The variation of A_{FB}^b with energy has been taken from ZFITTER predictions. To estimate its influence on the result, its value was varied by ± 0.030, corresponding to half the total predicted change of A_{FB}^b. The observed variation in A_{FB}^c is found to be less than 0.015. In principle the production rate of $D*$ mesons at energies off the peak has to be redetermined. However, as long as the relative production of $D*$ from c to $D*$ from b and the level of background does not change the result of the asymmetry fit is not affected. This c/b ratio has been investigated as a function of energy with the ZFITTER package. It changes by 7.5% between on peak energies and the extreme off peak energies. This introduces an additional uncertainty in the normalizations of the $D*$ production rates from b and c. Introducing this uncertainty into the fit results in an error of ± 0.010 for the asymmetries at the off peak points. A total systematic error of 0.03 has been assigned to the off peak points.

9 A combined determination of A_{FB}^c and A_{FB}^b using $D*$ mesons and leptons

In a recent publication [2] the OPAL collaboration has published a simultaneous measurement of A_{FB}^c and A_{FB}^b using prompt, energetic leptons in Z^0 decays. The results obtained from that analysis are:

$$A_{FB}^c = 0.014 \pm 0.030 \, (\text{stat.}) \pm 0.020 \, (\text{sys.}),$$

$$A_{FB}^b = 0.092 \pm 0.018 \, (\text{stat.}) \pm 0.007 \, (\text{sys.}) \pm 0.003 \, (\text{mix.}),$$

with a statistical correlation coefficient of $+0.29$. The third error on A_{FB}^b is the systematic error associated with $B\bar{B}$ mixing.

It should be noted that the leptons from charm and bottom quarks are oppositely charged, but the $D*$ from the two quarks have the same charge, implying that the correlation of the charm and bottom asymmetries is positive for leptons and negative for $D*$. This suggests that a combination of the two measurements could lead to a significant reduction in the correlation coefficient and the error.

Both measurements are combined taking into account the statistical and systematic errors listed in Table 4. The different errors have been split into correlated and uncorrelated errors. The χ^2 to be minimized is defined by

$$\chi^2 = \Delta \mathbf{A}_{FB}^T \cdot (\mathscr{C})^{-1} \cdot \Delta \mathbf{A}_{FB}, \tag{14}$$

where $\Delta \mathbf{A}_{FB}$ is the vector $(A_{FB}^{c,l} - A_{FB}^c, A_{FB}^{b,l} - A_{FB}^b, A_{FB}^{c,D*} - A_{FB}^c, A_{FB}^{b,D*} - A_{FB}^b)$ and $(\mathscr{C})$ is the covariance matrix. Its elements are given in Table 5. They have been calculated using correlation coefficients for both analyses

Table 4. List of systematic errors for the combined lepton-D^* analysis

Error source	ΔA_{FB}^c	ΔA_{FB}^b
Uncorrelated errors		
Lepton analysis		
Lepton ID	0.016	0.0024
Lepton branchings	0.007	0.0019
Detector effects	0.003	0.0016
Total error lepton	0.018	0.0035
D^* analysis		
Background	0.009	0.036
x_{D^*} scale	0.002	0.006
Detector effects	0.002	0.006
ζ_{D^*}	0.000	0.009
Total error D^*	0.008	0.038
Correlated errors		
Lepton analysis		
b-c fragmentation	0.007	0.0023
$B\bar{B}$ mixing	0.000	0.0060
D^* analysis		
b-c fragmentation	0.003	0.010
$B\bar{B}$ mixing	0.000	0.032

Table 5. Covariance matrix for the combination of the lepton and the D^* asymmetry measurement including all statistical and systematic errors

	$A_{FB}^{c,l}$	$A_{FB}^{b,l}$	A_{FB}^{c,D^*}	A_{FB}^{b,D^*}
$A_{FB}^{c,l}$	0.001303	0.00018	0.000021	0.000235
$A_{FB}^{b,l}$		0.00038	0.000019	0.000214
A_{FB}^{c,D^*}			0.002116	−0.003055
A_{FB}^{b,D^*}				0.01181

which include systematic errors. In the lepton analysis effects which change the relative fraction of $c\bar{c}$ and $b\bar{b}$ events in general lead to a negative correlation between A_{FB}^b and A_{FB}^c, while effects changing the overall fraction of prompt leptons lead to a positive correlation. Taking this into account a total correlation coefficient of $+0.251$ is found. The correlation coefficient including systematic errors for the D^* analysis is determined to be -0.623. In the calculation of the final error matrix full correlation has been assumed for the elements connecting both measurements. The statistical error of the combination has been determined by repeating this minimization after setting all elements in the convariance matrix correlating both measurements to zero and using only the statistical errors from the lepton and the D^* analysis.

The result of the combination is illustrated in Fig. 6, where the 1 σ total error ellipses, corresponding to a 37% confidence level, for the individual and the combined analyses are shown. Systematic errors are included in this plot. Also shown is the prediction of the Standard Model for top masses in the range between 80 to 250 GeV/c².
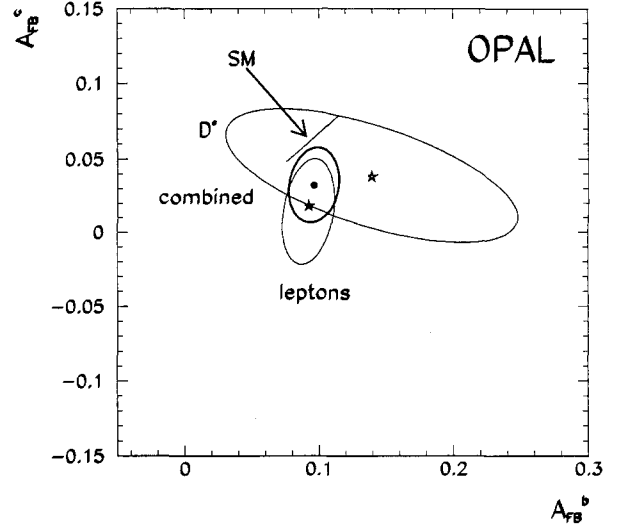
Fig. 6. Error ellipses for the asymmetries using prompt leptons, D^* mesons and the combined analysis. Shown are the 1σ contours corresponding to a 37% confidence contour, for the total errors, including statistical and systematic errors. The stars indicate the central values. The predicition of the Standard Model with a top mass between 80 GeV/c² and 250 GeV/c² is also shown. A variation of the Higgs boson mass between 50 and 1000 GeV/c² makes no visible difference

Varying the mass of the Higgs boson between 50 to 1000 GeV/c² makes no visible difference.

The final result of the combination of both measurements is

$$A_{FB}^c = 0.032 \pm 0.021 \,(\text{stat.}) \pm 0.015 \,(\text{sys.}),$$

$$A_{FB}^b = 0.096 \pm 0.017 \,(\text{stat.}) \pm 0.008 \,(\text{sys.}),$$

with the correlation coefficient of $+0.15$, significantly reduced compared to the individual measurements.

Using the JETSET model and predictions by ZFIT-TER corrections are calculated to translate these asymmetries into values at the Born level. The corrections are $A_{FB}^{c,0} = A_{FB}^c + 0.013 - 0.006$, $A_{FB}^{b,0} = A_{FB}^b + 0.008 - 0.002$, where $A_{FB}^{q,0}$ are the Born level asymmetries. The first correction quoted is due to initial and final state photon radiation and QCD effects, the second one is due to the difference between the nominal Z^0 mass and the energy at which the on-peak data were collected.

10 Results and summary

The forward-backward asymmetry of the process $e^+e^- \rightarrow c\bar{c}$ has been measured using 12 832 D^* candidate events containing 5560 signal events at energies on the peak of the Z^0 resonance, which were identified using charged D^* mesons. The result, obtained after correcting for the production of D^* mesons from b quarks, is

$$A_{FB}^c = 0.052 \pm 0.028 \,(\text{stat.}) \pm 0.012 \,(\text{sys.}),$$

$$91.0 \,\text{GeV} < E_{\text{cms}} < 91.6 \,\text{GeV}.$$

The average centre of mass energy of the events is 91.28 GeV. Repeating the procedure for events below and above the Z^0 peak the energy dependence of the forward-backward asymmetry of the process $e^+e^- \to c\bar{c}$ is investigated. The values found are

$$A_{FB}^c = -0.14 \pm 0.14\,(\text{stat.}) \pm 0.03\,(\text{sys.}),$$

$$88.4\,\text{GeV} < E_{\text{cms}} < 90.3\,\text{GeV},$$

$$A_{FB}^c = 0.18 \pm 0.12\,(\text{stat.}) \pm 0.03\,(\text{sys.}),$$

$$91.9\,\text{GeV} < E_{\text{cms}} < 93.8\,\text{GeV},$$

where the average energies are 89.75 GeV and 92.64 GeV, respectively. These measurements are consistent with the predictions of the Standard Model for the energy dependence of the asymmetry of the process $e^+e^- \to c\bar{c}$ at energies around the Z^0 pole.

Combining the results with a measurement of the c and b quark asymmetry using prompt leptons, a simultaneous determination of both asymmetries is performed. The correlations between the two asymmetries are significantly reduced. The following values are found for energies on the peak of the Z^0 resonance:

$$A_{FB}^c = 0.032 \pm 0.021\,(\text{stat.}) \pm 0.015\,(\text{sys.}),$$

$$A_{FB}^b = 0.096 \pm 0.017\,(\text{stat.}) \pm 0.008\,(\text{sys.}),$$

with a correlation coefficient of $+0.15$.

The results are in good agreement with the Standard Model predictions of $A_{FB}^c = 0.054$ and $A_{FB}^b = 0.094$, which were obtained using the program ZFITTER [25] at a centre of mass energy of 91.2 GeV, assuming a top mass of 130 GeV/c^2 and a Higgs boson mass of 300 GeV/c^2.

References

1. J.H. Kühn, P. Zerwas: In: Z^0 Physics at LEP1, G. Altarelli et al. (eds.), CERN Yellow report 89-08, Vol. 1 (1989)
2. OPAL Coll.: CERN PPE/93-78. To be published in Z. Phys. C
3. L3 Coll., B. Adeva et al.: Phys. Lett. B252 (1990) 713; ALEPH Coll., D. Decamp et al.: Phys. Lett. B263 (1991) 325; DELPHI Coll., P. Abreu et al.: Phys. Lett. B276 (1992) 536
4. OPAL Coll., G. Alexander et al.: Phys. Lett. B262 (1991) 341
5. OPAL Coll., K. Ahmet et al.: Nucl. Instrum. Methods A305 (1991) 275
6. O. Biebel et al.: Nucl. Instrum. Methods A323 (1992) 169
7. OPAL Coll., G. Alexander et al.: Z. Phys. C52 (1991) 175
8. M. Hauschild et al.: Nucl. Instrum. Methods A314 (1992) 74
9. T. Sjöstrand: Comput. Phys. Commun. 39 (1986) 347; T. Sjöstrand, M. Bengtsson: Comput. Phys. Commun. 43 (1987) 367; T. Sjöstrand: Int. J. Mod. Phys. A3 (1988) 751
10. C. Peterson et al.: Phys. Rev. D27 (1983) 105
11. see for example: A.G. Frodesen, O. Skjeggestad: Probability and statistics in particle physics. Universitetsforlaget Bergen-Oslo-Tromsø 1979
12. OPAL Coll.: CERN PPE/93-106, submitted to Z. Phys. C
13. Particle Data Group: Review of Particle Properties, Phys. Rev. B45 (1992) 1
14. CLEO Coll., D. Bortoletto et al.: Phys. Rev. D37 (1988) 1719; CLEO Coll., D. Bortoletto et al.: Phys. Rev. D39 (1989) 1471
15. OPAL Coll., P.D. Acton et al.: Z. Phys. C60 (1993) 579
16. J. Allison et al.: Nucl. Instrum. Methods A317 (1991) 47
17. OPAL Coll., M.Z. Akrawy et al.: Z. Phys. C47 (1990) 505
18. ARGUS Coll., H. Albrecht et al.: Z. Phys. C52 (1991) 353
19. CLEO Coll., D. Bortoletto et al.: Phys. Rev. D45 (1992) 21
20. Electroweak b physics at LEP. Presented by R. Tenchini at the XXVIIIth Recontre de Moriond
21. P. Mättig: Phys. Rep. 177 (1989) 141
22. ARGUS Coll., H. Albrecht et al.: DESY 92-050
23. CLEO Coll., J. Bartelt et al.: Cornell Report CLNS 93/1207, submitted to Phys. Rev. Lett.
24. I. Bigi, R. Rückl: private communications
25. Line shape program ZFITTER, version 451, including an implementation of $e^+e^- \to 4$ fermions. Dubna-Zeuthen radiative correction group, D. Bardin et al.: Comput. Phys. Commun. 59 (1990) 303; Z. Phys. C44 (1989) 493; Nucl. Phys. B351 (1991) 1; Phys. Lett. B229 (1989) 405; CERN-TH 92/6443